Observational Analyses of Dramatic Developments of A Severe Air Pollution Event in the Beijing Area

Ju Li[1], Jielun Sun[2], Mingyu Zhou[3], Zhigang Cheng[1], Qingchun Li[1], Xiaoyan Cao[1], and Jingjiang Zhang[1]

[1]Institute of Urban Meteorology, China Meteorological Administration, Beijing 100089, China
[2]National Center for Atmospheric Research, Boulder, Colorado, USA
[3]National Marine Environment Forecast Center, Beijing, China

Correspondence to: Jielun Sun (jsun@ucar.edu)

Abstract. A rapid development of a severe air pollution event at Beijing, China at the end of November 2015 was investigated with observations collected during the Study of Urban Rainfall and Fog/Haze (SURF-15). The analyses indicate that the major pollution source associated with particulate matter of diameter 2.5 μm ($PM_{2.5}$) was from south of Beijing. On the night of 29 November, the surface stable boundary layer (SBL) was formed northwest of Beijing due to the northwesterly

5 wind downslope of the mountains surrounding Beijing. This relatively cold and less polluted air also diluted the surface air northwest of Beijing while in the southeast of Beijing, the $PM_{2.5}$ concentration increased continuously through the transport of the surface southwest flow. Around the midnight, the wind above the SBL switched from northerly to southwesterly and transported the heavy polluted air over Beijing. As the daytime convective turbulent mixing developed in the morning of 30 November, turbulent mixing transported the upper polluted air downward, leading to the dramatic increase of the $PM_{2.5}$

10 concentration in the urban area. Meanwhile, the daytime weakly northeast-east surface wind led to the horizontal transport of the high $PM_{2.5}$ air westwards towards Beijing, which further enhanced the $PM_{2.5}$ increase at Beijing. As a result of both turbulent mixing and advection with possible aerosol growth from secondary aerosol formation under the low wind and high humidity conditions, the $PM_{2.5}$ concentration reached over 700 μg m^{-3} at Beijing by the end of 30 November. Contributions of the two transporting processes to the $PM_{2.5}$ oscillations prior to this dramatic event were also analyzed.

1 Introduction

Currently China is one of the fast-growing-economy countries in the world. Its rapid urbanization leads to heavy air pollution, which has drawn broad attention worldwide. Although the number of "blue sky" days measured by the air quality index (AQI) in 2015 increased from its 2014 number according to the state bulletin issued by the Chinese Ministry of Environmental Protection (Chinese EPA), air pollution is still a serious issue especially in the region of Beijing-Tianjin-Hebei (BTH) and its

20 surrounding area including provinces of Shanxi, Shandong, Henan, and Inner Mongolia. Heavy pollution have occurred in 70 large Chinese cities, which covers 44.1% of China. In 2015, 13 cities in the region of BTH that are monitored by the Chinese EPA failed to meet the Chinese air quality standard for 47.6% of the year. Light, medium, heavy, and severe pollution days for these cities occurred 27.1%, 10.5%, 6.8% and 3.2% of the year, respectively.

Air pollution occurrence frequency, intensity, and impact areas are major concerns in China (Wang et al., 2014b). The worst pollution season at Beijing is during fall and winter between October and March. An increasing number of studies have focused on Chinese air pollution and haze issues. Meng and Cheng (2002) found that heavy pollution in Beijing is often associated with surface low pressures. Using backward trajectory analysis, Zhang et al. (2007) found that although easterly

5 flows occur only 12% of winter time, they are highly correlated with heavy pollution events. Liao et al. (2015) reviewed air pollution mechanisms and found that the complex terrain in the region of BTH is one of the important contributing factors to air pollution in the region. They also pointed out that the bow-shaped mountains in the northwest of Beijing often block and weaken cold air from northwest and create a stagnant airshed with pollutants and water vapor trapped for haze and fog formation in Beijing. Local circulations thermally and mechanically forced by the mountains, land-sea contrasts from Bohai

10 east of Beijing, and urban canopies also contribute air pollution transportation in the Beijing area (e.g., Xu et al., 2005; Chen et al., 2009; Liu et al., 2009).

Zhang et al. (2006), Zhang et al. (2012), and Zhao et al. (2013) indicated that the planetary boundary layer (PBL) depth is associated with the volume for pollutants to expand; low PBLs provide favorite conditions for development of heavy pollution events. Wang et al. (2014a) reported that explosively developed and long-lasting air pollution events in Beijing are commonly

15 associated with weak surface highs or lows with weak winds, stable boundary layers (SBL), and high humidity. They also pointed out that rapid disappearance of air pollutants is commonly associated with strong northernly winds from a surface high pressure centered west of Beijing.

Human activities contribute increased water vapor release in urban areas compared to rural areas. Han and Zhang (2014) found relative humidity about 10% to 40% higher than the annual average value is often connected with heavy pollution events

20 at Beijing and its surrounding provinces. Zhang et al. (2012) investigated high-humidity enhancement of hygroscopic growth of aerosols. Sun et al. (2014) found that high humidity could also enhance heterogeneous chemical reactions with highly concentrated mineral particles to increase generation of secondary aerosols. Quan et al. (2014) found that during heavy pollution events, significant amounts of NO_3 and SO_4 particles can be produced by gas-particle transformation from NO_x and SO_2. Overall, increased aerosol concentrations reduce visibility and lead to apparent concentration increases of particulate matter

25 with diameter 2.5 μm ($PM_{2.5}$) and air pollution (e.g., Dou et al., 2014). Due to lack of spatial meteorological and chemical observations covering the BTH region especially in vertical, it is difficult to understand mechanism of haze formation in terms of interactions between pollution sources, pollutant distribution, atmospheric physical-chemical processes, and boundary layer influences.

During the seven-days period between 26 November and 2 December 2015, an extremely heavy pollution event with the

30 daily mean AQI greater than 200 developed in Beijing. The event would be classified as "red alert" by the Chinese EPA. However based on the local forecast, the pollution intensity of "orange alert" was issued instead. The failure of issuing the correct warning was publicized widely. During this event, the $PM_{2.5}$ concentration oscillated dramatically 12 hours before the final rapid increase on 30 November (Fan et al., 2015). This event happened to occur during the three-year field campaign of the Study of Urban Rainfall and Fog/Haze (SURF-15) (Liang et al., 2017), which started in the spring of 2015. Using extra

35 measurements from SURF-15 as well as routine measurements spread around Beijing described in section 2, we investigate

physical processes that led to the heavy pollution event in this study. We first study the regional environment related to the development of the heavy pollution event in section 3. We then examine physical transporting processes responsible for the dramatic oscillations of $PM_{2.5}$ prior to and in the development of the rapid increase of $PM_{2.5}$ on 30 November in section 4. Summarizes are in section 5.

2   Instrumentation and Observations

The observations (http://www.ium.cn:8088/dataCenter/) were collected during SURF-15 sponsored by Institute of Urban Meteorology (IUM). We mainly focus on the data collected at the research site operated by the Institute of Atmospheric Physics (IAP), Chinese Academy of Sciences. All the observation heights described in this section are above the ground level (AGL). At the IAP site, a 325-m research tower has been operational since 1978. Wind directions (020C, American MetOne) and speeds (010C, American MetOne), air temperature, and relative humidity (HC2-S3, Rotronic, Swiss) were measured at 15 levels (8, 15, 32, 47, 65, 80, 100, 120, 140, 160, 180, 200, 240, 280, 320 m) on the tower with the sampling rate of one sample per 20 s and averaged to one per min. Wind speeds at each level were measured on two booms: one pointed to 315 deg from north and the other one to 135 deg; the larger value of the two is chosen as the wind speed for the level. Wind directions were only measured by one sensor at each level. Three-dimensional sonic anemometers—each on a 2.2 m boom from the tower center—were installed at 47 m (Windmaster, Gill), 140 m (CSAT3, Campbell Scientific), and 280 m (CSAT3, Campbell Scientific) at the direction of 30°, 210°, and 230° relative to the center of the tower, respectively. Downward and upward pointing pyrgeometers and pyranometers (CNR1, Kipp & Zonen), and sensors for CO_2 and H_2O concentrations (LI-7500) were also installed at these three levels. The data from the sonic anemometers and the LI-7500's were sampled at 10 samples per second. The turbulence data were calculated at 30-min segments using the EDDY-PRO software (Burba, 2013). We also use the surface station about 20 m south of the IAP tower, where wind speed and direction (05103-L, R. M. Young), and temperature and relatively humidity (HMP45C, Vaisala) at 2.2 m were measured at one sample per 2 s.

In addition, a Doppler lidar (Windcube 100S, Leosphere) and a mini-micropulse aerosol lidar (mini-MPL, SigmaSpace) were located at about 20 m west-northwest of the IAP tower; the two lidars were 3-m apart. To observe wind profiles, the Doppler Beam Swing (DBS) mode was used at 5 s intervals with the vertical resolution of 20 m (Campbell et al., 2002), and the data were averaged to 1 min segments. Due to the optical overlap function issue (Hey et al., 2011), the lowest Doppler lidar observation height was set to 70 m based on comparison between lidar and in-situ observations even though its first range gate labeled by the manufacturer is 50 m. The carrier-to-noise ratio (CNR), which is found to be highly correlated with aerosol backscatter (Aitken et al., 2012), as well as wind speeds and directions were observed from the Doppler lidar. Normalized relative backscatters (NRB) were derived from the mini MPL lidar measurement with the sampling rate of one sample per 30 s and the vertical resolution of 30 m above 100 m.

Furthermore, we use remote sensed measurements from a mini-MPL at IUM, the ceilometer lidar (CL51) at Finnish Embassy (FIN), a wind profiler (CFL-08) at Nanjiao Guanxiang Tai (NGT) and Haidian (HAI) located 7 km to the northwest of the IAP tower (all these locations are marked on Fig. 1). We also use radio soundings launched twice a day at NGT, which is about

20 km southeast of the IAP tower. During the study period, daily MODIS (Moderate Resolution Imaging Spectroradiometer) Rapid Response satellite images over the Beijing Area are available from AERONET (https://aeronet.gsfc.nasa.gov/).

From the dense network of automatic weather stations (AWS) operated by Beijing Meteorological Service (BMS), we also use measurements of wind speed and direction (EL15-2C) at 10 m, temperature and humidity (HMP155, Chinese Huayun Company) at 1.5 m, and pressure (PTB210, Chinese Huayun Company) at 1.5 m observed at Changping (CHP), Chaoyang (CHA), Mentougou (MEN), Daxing (DAX), Tongzhou (TON) and HAI. In addition, we also use the hourly $PM_{2.5}$ concentration measured at ~ 2 m at these stations operated by BMS as part of their air quality monitoring network and the $PM_{2.5}$ concentration at the IAP site measured at ~ 10 m every minute. The $PM_{2.5}$ concentration was measured with LGH-01E, Landun Photoelectron Company at HAI, MEN, and TON, with Grimm 180 at CHA, CHP, and DAX, and with Thermo SHARP5030 at IAP.

3   Regional environment at Beijing and its surrounding area

Starting on 26 November, the $PM_{2.5}$ concentration started to increase steadily (Fig. 2). From 0500 LST, 30 November, the $PM_{2.5}$ concentration increased dramatically and reached 732 μg m^{-3} at HAI and 786 μg m^{-3} at MEN at 1500 LST on 1 December.

From 29 to 30 November, a weak high pressure ridge at 850-mb moved from west to east of Beijing (Fig. 3). Because of the movement of this pressure ridge, the wind at the upper PBL changed from northwesterly on 29 November to southwesterly on 30 November, which is consistent with the sounding observations at NGT (Fig. 4). The wind profiler observations at both NGT and HAI indicate that the wind direction change occurred around the midnight of 29 November (Fig. 4). On the surface, Beijing was between a high pressure on the northwest and a low pressure on the southeast on 29 November, which resulted in the easterly flow in Beijing, and was between a weak high pressure on the east and a low pressure on the west on 30 November, which resulted in weak northeast winds in the lower PBL (Fig. 3).

The 2000-LST sounding at NGT on 29 November shows that there was a well-mixed layer above about 200 m up to about 1800 m indicating that the convective turbulent mixing during the daytime of 29 November was relatively strong. The 0800-LST sounding on 30 November indicates that a well mixed convective boundary layer (CBL) started to develop near the surface with the overnight SBL above and being entrained into the CBL. The relatively well-mixed residual layer from the previous daytime mixing was above the elevated stable layer (Fig. 4). The CBL on 30 November was associated with weak northeast winds, and the stable layer above was dominated by southwest winds. The relative humidity was higher in the stable layer than the residual layer above and the newly developed CBL below. Within the stable layer, the relative humidity decreased with height and dropped sharply at the bottom due to the turbulent mixing in the CBL below. By 2000 LST on 30 November, the surface layer changed to a SBL of near 100 m with the daytime well-mixed convective air above. The wind direction in the daytime convective layer became southernly and the bottom SBL was northeasterly to easterly. In addition, the air humidity increased in both the SBL and the daytime convective layer above. The increased humidity is consistent with the reported visibility of less than 1 km at most AWS stations around Beijing on 30 November.

At 0000 LST, 30 November, the surface $PM_{2.5}$ concentration was high south of Beijing (Fig. 5). This polluted air was visibly confined east of the Taihang Mountain Ridge from the MODIS images on 29 and 30 November (Fig. 6). During the early morning hours of 30 November, the high surface $PM_{2.5}$ concentration center was shifted toward the southeast of Beijing with its maximum value increased (Fig. 5). The observation of the relatively strong northwest-north wind at MEN west of Beijing prior to the rest of the surface stations has characteristics of the downslope flow. The relatively clean downslope flow reduced the surface $PM_{2.5}$ concentration northwest of Beijing. As a result, the high surface $PM_{2.5}$ concentration was "moved" to be southwest of Beijing. As the CBL grew after sunrise, the high $PM_{2.5}$ air was moved northeastward following the wind direction above the CBL (Fig. 5), indicating that the vertical coupling between the surface layer and the upper polluted air during the daytime (see detailed analyses in next section). Meanwhile, the $PM_{2.5}$ concentration at Beijing increased dramatically from 0500 LST to 1100 LST, and its development was faster than its surrounding area (Fig. 5), for which, the rough surface of the urban area might have contributed additional turbulent mixing (Sun et al., 2017).

4 Physical transporting processes in development of the heavy pollution event at Beijing

In general, turbulence is generated either by positive buoyancy or by shear. Turbulent mixing leads to vertical transports of heat from the diurnal heating and cooling of the surface, resulting in air temperature changes. The vertical momentum transfer also changes wind speed and direction because the background wind changes with height especially near the surface. Turbulent mixing during daytime is commonly generated by convection, especially under weak winds, resulting from the heated air at the surface through molecular thermal conduction at the interface between the air and the ground heated by downward solar radiation. Once wind speeds are high, wind shear near the surface can also generate turbulence, which can occur day and night although shear is the dominant turbulence generation mechanism at night. At night, the air near the surface is cooled by molecular thermal conduction from the cold surface due to the longwave emission. The vertical temperature difference between the warm air heated from the daytime and the cooled air near the surface leads to the SBL, which reduces turbulence intensity and vertical turbulent transports of momentum, heat, trace gases and aerosols. As a result, the air-surface coupling and the surface emitted trace gases of water vapor and CO_2 are confined near the surface. Impacts of the surface roughness on air motions are also limited to the near-surface stable layer (e.g., Sun et al., 2016). In summary, the diurnal variation of the solar radiation leads to the diurnal variation of air temperature, wind speed and direction, trace gases, and aerosols.

During the first three days of our study period, 26-28 November, the maximum downward solar radiation decreased steadily (Fig. 7a). The low downward solar radiation on 28 November was consistent with the cloudy MODIS satellite image that day (Fig. 6a). The $PM_{2.5}$ concentration, air potential temperature θ, specific humidity q, and CO_2 increased steadily with their diurnal variations associated with turbulent mixing embedded in their temporal variations (Fig. 7). The wind speed was high during the first part of 26 November, and was low for the rest of the three days (Fig. 7g), which was consistent with the decreasing pressure observed at IAP (Fig. 7e). The wind direction within the IAP tower layer varied diurnally especially when the ambient wind speed was low on 27 and 28 November (Fig. 7f); it was from west in the first half of each day and from east during the second half of each day, indicating the mountain west of Beijing played a role in the diurnal wind direction change.

Because of the contribution of the positive buoyancy to turbulent mixing during daytime, turbulence intensity represented by the standard deviation of the vertical velocity σ_w increased during daytime on 27 and 28 November even though the maximum downward solar radiation was relatively low on 28 November (Fig. 7h). Because the weak pressure system over Beijing, the diurnal variation of wind speed was not dramatic and the vertical variation of wind speed within several hundreds of meters
5 above the surface was relatively small.

The $PM_{2.5}$ concentration at IAP went through significant oscillations before its final dramatic increase on 30 November (Fig. 8a). Right after the noon of 29 November, the $PM_{2.5}$ concentration decreased significantly until about 1800 LST (marked stage 1 in Fig. 8). After sunset, the $PM_{2.5}$ concentration increased to its temporal maximum value around 2200 LST (marked 2 in Fig. 8). Then it decreased sharply until the early morning of 30 November (marked 3 in Fig. 8). Around 0600 LST, the
10 $PM_{2.5}$ concentration started its steady dramatic increase toward its highest value of the day, 527 $\mu g\ m^{-3}$, around 2000 LST (marked 4 in Fig. 8). Then the $PM_{2.5}$ concentration reached to a relatively steady state; the $PM_{2.5}$ concentration varied $\pm$ 100 $\mu g\ m^{-3}$ until the night of 1 December when it decreased to below 50 $\mu g\ m^{-3}$.

We find that both turbulent mixing and advection contribute the up and down of the $PM_{2.5}$ concentration at IAP between the noon of 29 November and the midnight of 30 November. In the rest of this section, we analyze the $PM_{2.5}$ oscillations
15 marked as four stages in Fig. 8. We also analyze the steady high $PM_{2.5}$ period from the night of 30 November through most of 1 December, and the final dramatic reduction of the high $PM_{2.5}$ concentration around the midnight of 1 December.

4.0.1 Stage 1

On 29 November, the downward solar radiation measured at IAP was significantly larger than the previous cloudy day (Fig. 7a). The convective mixing increased in the morning as shown in both σ_w and turbulence kinetic energy (TKE) (marked 1 in
20 Figs. 8d and 8e). Normally the convective turbulent mixing in the morning would vertically spread trace gases and aerosols accumulated in the nighttime SBL, leading to reduction of their concentrations. However in this morning, the lower level wind was from south (Fig. 8f), where the pollution was heavy. As a result of the transport of the polluted air from south, the concentrations of $PM_{2.5}$, q, and CO_2 increased slightly (Figs. 8a, 8b, and 8c) until the increase of the strong northwesterly wind arrived in the afternoon (Fig. 8g). The strong wind shear relative to the rough urban surface generated strong turbulent
25 mixing (e.g., Sun et al., 2017), and resulted in the strong upward transport of the polluted air and the downward transport of the less-polluted air from northwest, leading to the decrease of $PM_{2.5}$, q, and CO_2 (marked 1 in Figs.8a, 8b, and 8c). Thus, the shear-generated turbulent mixing contributed the reduction of the surface $PM_{2.5}$ concentration in the afternoon of 29 November.

4.0.2 Stage 2

Because of the strong heating during the daytime of 29 November, the air temperature was the highest during the 7-day
30 period (Fig. 7b). When the downward solar radiation decreased in the afternoon, the reduced solar heating at the surface and the emission of the longwave radiative from the surface resulted in the surface cooling. Molecular thermal conduction at the cooling surface led to the air temperature decrease near the surface while the air above was still relatively warm from the daytime heating. Consequently the vertical air temperature difference became significant especially after the downward

solar radiation approached zero after sunset (marked 2 in Fig. 8h), leading to the SBL (Fig. 8i). Because of the strong stable stratification near the surface, the shear-generated turbulence near the surface was reduced significantly from its daytime value. The weak turbulent mixing under the very SBL constrained the vertical spreading of the surface trace gases and aerosols. Meanwhile, the wind direction near the surface started to be influenced by the mountains northwest of Beijing. During the

5   development of the downslope wind, the wind within the tower layer changed gradually from easterly to northwesterly. As the wind direction changed to southerly, the flow transported the polluted air into Beijing. Because the nighttime SBL prevented the air with high aerosol, q and CO_2 from being mixed up, the $PM_{2.5}$ concentration as well as q and CO_2 increased sharply (marked 2 in Figs. 8a, 8b, and 8c).

4.0.3   Stage 3

10 Because the thermally induced terrain flow is due to the horizontal pressure gradient generated by the daytime heating and the nighttime cooling over the sloped terrain similar to land breezes (Sun et al., 1998), the relatively strong heating on 29 November would lead to the relatively strong downslope drainage flow. Under the influence of the relatively clean downslope flow, the $PM_{2.5}$ concentration in the vicinity of the mountains northwest of Beijing was reduced, and the high $PM_{2.5}$ concentration center was moved to southeast of Beijing (Fig. 2) starting around 0000 LST on 30 November. Because of the spatial variation

15 of the downslope flow, the temporal variation of $PM_{2.5}$ varied spatially (Fig. 2).

The decoupling associated with the strong stable stratification as a result of the large solar heating prior to the night also reduced the influence of the rough surface on slowing the air flow above. As a result, the wind speed at 140 m and 280 m above the SBL increased in the early morning of 30 November (marked 3 in Fig. 8g). Meanwhile, the surface wind direction changed to northeasterly under the influence of the surface pressure system (marked 3 in Fig. 8f), which brought in the less-polluted

20 air. The increased wind speed from northeast led to the increased turbulent mixing and the vertical spreading of the polluted surface air (Figs. 8d and 8e). Therefore, both the advection of the less polluted air into the Beijing urban area and the small increase of turbulent mixing in the vertical spreading of the polluted air near the surface below the upper-level southwesterly flow contributed the significant decrease of the $PM_{2.5}$ concentration at IAP in the early morning of 30 November (Fig. 8a). The transporting processes also decreased the concentration of q and CO_2 (marked 3 in Figs. 8b and 8c).

25 Similar to stage 2, the temporal variation of the $PM_{2.5}$ concentration varied spatially at this stage as the nighttime boundary layer was strongly influenced by the spatially varying downslope flow (Fig. 9). The $PM_{2.5}$ concentration at the most western station, MEN, started to decrease first in the early evening and lasted the longest until nearly noon on 30 November. In contrast, the $PM_{2.5}$ concentration at southeast of Beijing, TON, which is far from the mountains, remained around 500 $\mu g\ m^{-3}$ from the night of 29 November until the early moring of 30 November (Fig. 9). As downslope flows transported air from the relatively

30 high elevation where the air humidity was lower, the relatively large humidity and the high $PM_{2.5}$ concentration at TON in the evening of 29 November further indicates that the downslope wind did not influence TON much. In the early morning of 30 November, both the q and the $PM_{2.5}$ concentrations at TON decreased slightly in response to the wind direction change while the wind speed remained weak (Fig. 9), suggesting that the horizontal advection contributed to the q and the $PM_{2.5}$ changes in the morning.

While the surface $PM_{2.5}$ concentration at IAP decreased in the morning of 30 November, the wind direction above the tower changed from northwest to southwest around the midnight of 29 November (Fig. 4). The strong decoupling between the SBL and the upper air also helped the upper-level southwest wind transporting the polluted air from south to above Beijing urban area efficiently without being mixed down to the surface (Fig. 10). The aerosol lidars associated with the relatively high backscatter density at FIN and the relatively high NRB at IUM and IAP, and the Doppler lidar associated with the relatively high CNR at IAP all show that the elevated high aerosol layer, which came down to about 300 m in the early morning of 30 November before 0600 LST.

4.0.4 Stage 4

In the morning of 30 November, the heavy polluted air above was efficiently transported by the southwesterly flow due to its decoupling from the rough surface, which ended up with the elevated polluted air above the surface SBL as shown in the lidar observations (Fig. 10). The close correlation between the Doppler CNR and the mini MPL NRB for high aerosol concentration is clearly demonstrated at 270 m between 0600 LST and 0700 LST on 30 November (Figs. 10a and 10b). The altitude of the high CNR observation in the early morning of 30 November indicates that the high aerosol layer was spreading by the relatively strong southeast wind in the residual layer above the relatively thin SBL, which became to be influenced by northeasterly winds in the morning. The elevated aerosol layer is consistent with the elevated humid air observed from the soundings at NGT because the polluted air from south is characterized with high humidity and high $PM_{2.5}$ concentration (Fig. 4). The absence of the elevated NRB between 0700 and 1000 LST at IAP could be due to the fast decrease of the lidar power with distance from the Doppler lidar (Davoust et al., 2014).

After the downward solar radiation increased in the morning of 30 November (marked 4 in Fig. 8a), the convective mixing increased as shown in both σ_w and TKE (marked 4 in Figs. 8d and 8e). The enhanced convective mixing resulted in the coupling between the surface and the elevated polluted air, which transported the heavy polluted air downward and the less polluted air upward and led to the steady increase of the $PM_{2.5}$ concentration, air temperature, wind speed, q, and CO_2 within the CBL in the morning (marked 4 in Fig. 8).

Because the growth of the CBL and the southwesterly flow above the CBL, the high aerosol layer appeared to be "lifted" gradually from 270 m to about 400 m between 0600 and 1200 LST on 30 November even though the entrainment of the polluted air into the CBL reduced the aerosol concentration right above the CBL. Because the relatively shallow CBL at its beginning development, the aerosol concentration in the CBL below the elevated high aerosol layer increased dramatically. As the CBL kept on growing, the high aerosol air was completely engulfed into the CBL around 1100 LST, leading to the explosive increase of the $PM_{2.5}$ concentration.

The connection between the CBL development and the $PM_{2.5}$ increase is also visible in the correlation between the increase of the downward solar radiation, which drives the CBL, and the increase of the $PM_{2.5}$ concentration in Fig. 8a. Because of the overwhelming coverage of concrete large surface elements in the urban area, the CBL developed faster over the urban area than the rural area, leading to the fast downward transport of the polluted air as shown at 0900 LST and 1100 LST in Fig. 5.

The convective coupling between the surface and the upper air also led to the significant increase of the $PM_{2.5}$ concentration east of Beijing where the surface $PM_{2.5}$ concentration was higher than that at the Beijing urban area (Fig. 5). As the downward solar radiation started to decrease, the air layer near the surface started to become stable again while the upper level convective mixing was still going on. The northeasterly wind within the CBL helped the horizontal advection of the polluted air toward IAP, which further enhanced the increase of the $PM_{2.5}$ concentration as shown in both Fig. 10a and Fig. 8a. In the end, within eight hours from 0900 to 1700 on 30 November, the $PM_{2.5}$ concentration increased about 450 $\mu g\ m^{-3}$ at IAP.

Based on previous studies in the region and around the world, the stagnant urban environment with increasing humidity and anthropogenic emissions of volatile organic compounds, nitrogen oxides, and sulfur dioxides provide favorable conditions for aerosol growth and secondary aerosol formation as a result of chemical reactions and hygroscopic growth of aerosols (e.g., Mader et al., 1952; Van Dingenen et al., 2004; Putaud et al., 2004, 2010; Parrish et al., 2011; Guo et al., 2014; Zhang et al., 2015). Therefore, aerosol growth might have also contributed the dramatic increase of the $PM_{2.5}$ concentration on 30 November. As a result, the maximum downward solar radiation on 30 November was only about a half of the one on 29 November.

4.0.5 The period of the steady high $PM_{2.5}$ and its rapid depletion

Around the midnight of 30 November, the air flow in the tower layer changed direction from northeasterly to northwesterly and the wind speed within the tower layer increased slightly under the influence of the mountain west and north of Beijing (Figs. 8f and 8g). The wind direction change brought in the less polluted air, resulting in the surface $PM_{2.5}$ concentration reduction of about 100 $\mu g\ m^{-3}$. Meanwhile, clouds moved in as indicated in the time series of the downward longwave radiation (not shown) and the MODIS image around noon (Fig. 6d), which results in the near zero downward solar radiation at the surface. Without wind shear and surface heating to generate turbulent mixing to transport the heavy polluted air vertically and without effective horizontal advection to reduce the pollutant concentration, the heavy polluted air remained in the weakly stable urban boundary layer. Because the air was nearly saturated during the entire day of 1 December, the aerosol growth might be limited. The high $PM_{2.5}$ air of about 500 $\mu g\ m^{-3}$ at IAP lasted throughout the daytime of 1 December until the significant increase of northwesterly wind arrived at the midnight, which reduced the $PM_{2.5}$ concentration down to below 50 $\mu g\ m^{-3}$ within two hours.

Overall, both turbulent mixing and advection are responsible for transporting the high-polluted air to the Beijing urban area and the $PM_{2.5}$ oscillations. Turbulent mixing is to transport pollutants from high to low concentration areas. If the upper level concentration of a pollutant is low, vertical turbulent mixing would lead to the decrease of the surface concentration. If the vertical concentration gradient is reversed, vertical turbulent mixing leads to an increase of the surface concentration. Vertical turbulent mixing needs either surface heating or wind shear. Advection is to transport the air downstream. If the concentration of a pollutant is higher upstream than downstream, the downstream pollutant concentration would increase. In contrast to turbulent mixing, the downstream concentration would not affect the upstream concentration effectively. Horizontal advection requires an air flow and a concentration difference between upstream and downstream. The roles of turbulent mixing and advection in the development of the severe air pollution event are schematically illustrated in Figure 11.

5 Conclusions

We analyzed the extreme heavy pollution event at the end of November 2015, Beijing, China based on the observations collected during SURF-15. We found that both turbulent mixing and horizontal advection contributed to the transport of the pollutants originated mainly south of Beijing.

Because of the regional pressure system, the flow above the PBL was mainly from northwest and southwest before and after the midnight of 29 November, respectively, and the bottom of the PBL flow varied diurnally between nighttime northwesterly under the influence of the mountain northwest of Beijing and daytime northeasterly. Diurnal variations of turbulent mixing and terrain thermally induced surface flows as well as the synoptic pressure system changes resulted in significant oscillations of the surface $PM_{2.5}$ concentration prior to and the dramatic increase of $PM_{2.5}$ on 30 November.

During the daytime of 29 November, the relatively strong downward solar radiation led to the significant warming of the boundary layer air. As the surface cooled down from the longwave radiative emission and the reduced downward solar radiation in the afternoon, the cooled surface air and the upper-level warm air resulted from the daytime warming transformed the surface layer into the stable boundary layer. In addition, the surface flow downslope of the mountains northwest of Beijing brought in the relatively cold air, which further strengthened the surface stable boundary layer. As the downslope flow from northwest was less polluted, the surface $PM_{2.5}$ concentration under the influence of the downslope flow was reduced in the northwest part of Beijing and the high $PM_{2.5}$ concentration appeared in the southeast part of Beijing. Around the midnight of 29 November, the upper wind changed from northwest-north to southwest. The southwesterly wind above the stable boundary layer effectively transported the polluted air south of Beijing to above the urban area as the stable boundary layer decoupled the rough surface from the upper flow.

After sunrise, the daytime convective mixing with large coherent eddies transported the elevated polluted air downward, which initiated the dramatic increase of the surface $PM_{2.5}$ concentration in the morning of 30 November. Meanwhile, the vertical mixing of the polluted air transported by the upper southwesterly flow also increased the surface $PM_{2.5}$ east of Beijing, which had higher $PM_{2.5}$ concentration than the value at Beijing. The daytime weakly northeast surface wind advected high $PM_{2.5}$ air into Beijing, which further enhanced the dramatic increase of $PM_{2.5}$ at Beijing in the afternoon until the midnight when the $PM_{2.5}$ reached over 700 μg m^{-3}. The efficient advective transport in the afternoon is associated with the reduced convective mixing by the development of the surface stable boundary layer and the weak shear-generated turbulent mixing associated with the weak environmental horizontal pressure gradient. Therefore, the dynamic transporting processes from both advection and turbulent mixing led to the dramatic increase of $PM_{2.5}$ at Beijing on 30 November. The cloud cover on 1 December prevented buoyancy-generation of turbulence and weak winds prevented shear-generation of turbulence, leading to the stagnant high $PM_{2.5}$ air throughout 1 December until the midnight of 1 December when the strong northwesterly wind arrived, which reduced the $PM_{2.5}$ concentration to below 50 μg m^{-3} at Beijing. The low wind and high humidity air during the build-up of the polluted air might have also contribute aerosol growth.

Data availability. http://www.ium.cn:8088/dataCenter/

Competing interests. The authors declare that they have no conflict of interest

Acknowledgements. The authors would like to acknowledge the data collected by the IAP, Chinese Academy of Sciences. The SURF project
is sponsored by Institute of Urban Meteorology, Meteorological Administration, Beijing, China, the Ministry of Science and Technology of
5   China, Grant numbers 2015DFA20870 and 2016YFC0203302, the National Natural Science Foundation of China, Project No. 41505102,
and Beijing Natural Science Foundation of China Grant No. 8171002. The University Corporation for Atmospheric Research manages the
National Center for Atmospheric Research under sponsorship by the National Science Foundation. Any opinions, findings and conclusions,
or recommendations expressed in this publication are those of the authors and do not necessarily reflect the views of the National Science
Foundation.

References

Aitken, M. L., Rhodes, M. E., and Lundquist, J. K.: Performance of a wind-profile lidar in the region of wind turbine rotor disks, J. Atmos. Oceanic Technol., 29, 347–355, 2012.

Burba, G.: Eddy covariance method for scientifc, industrial, agricultural, and regulatory applications: A field book on measuring ecosystem
5   gas exchange and areal emission rates., LI-COR Bioscience, Lincoln, NE, USA, 2013.

Campbell, J. R., Hlavka, D. L., Welton, E. J., Flynn, C. J., Turner, D. D., Spinhirne, J. D., Scott III, V. S., and Hwang, I.: Full-time, eye-safe cloud and aerosol lidar observation at atmospheric radiation measurement program sites: Instruments and data processing, J. Atmos. Oceanic Technol., 19, 431–442, 2002.

Chen, Y., Zhao, C., Zhang, Q., Deng, Z., Huang, M., and Ma, X.: Aircraft study of mountain chimney effect of Beijing, China, J. Geophys.
10   Res., 114, 2009.

Davoust, S., Jehu, A., Bouillet, M., Bardon, M., Vercherin, B., Scholbrock, A., Fleming, P., and Wright, A.: Assessment and optimization of lidar measurement availability for wind turbine control, in: Scientific. Proceedings of EWEA Conference March, pp. 10–13, 2014.

Dou, J., Wang, Y., and Miao, S.: Characteristics of spatial and temporal structures of surface moisture and wind fields in Beijing area, Applied Meteorology Report, 25(5), 559–569, 2014.

15 Fan, M., Zhu, R., Zhu, K., and Li, Z.: Numerical simulation investigations of a lasting heavy air pollution event in the area of Beijing, Tianjin, and Hebei in November 2015, Plateau and Mountain Meteorology Research (in Chinese), 36, 7–14, 2015.

Guo, S., Hu, M., Zamora, M. L., Peng, J., Shang, D., Zheng, J., Du, Z., Wu, Z., Shao, M., Zeng, L., et al.: Elucidating severe urban haze formation in China, Proceedings of the National Academy of Sciences, 111, 17 373–17 378, 2014.

Han, X. and Zhang, M.: Model analysis of haze formation over the North China Plain in January, Clim. and Env. Res. (in Chinese), 19,
20   127–139, 2014.

Hey, J. V., Coupland, J., Foo, M. H., Richards, J., and Sandford, A.: Determination of overlap in lidar systems, Applied Optics, 50, 5791–5797, 2011.

Liang, X., Miao, S., Li, J., Bornstein, R., Zhang, X., Gao, Y., Cao, X., Chen, F., Cheng, Z., Clements, C., Debberdt, W., Ding, A., Ding, D., Dou, J. J., Dou, J. X., Dou, Y., Grimoond, C. S. B., Gonzalez-Cruz, J., He, J., Huang, M., Ju, S., Li, Q., Niyogi, D., Quan, J., Sun, J., Sun,
25   J. Z., Yu, M., Zhang, J., Zhang, Y., Zhao, X., Zheng, Z., and Zhou, M.: SURF: Understanding and Predicting Urban Convection and Haze, Submitted to Bull. Am. Meteor. Soc., x, x, 2017.

Liao, X., Zhang, X., and Wang, Y.: Comparisons of environmental conditions for long-lasting pollution events in Beijing between winter and summer, Environmental Science, 35(6), 2031–2044, 2015.

Liu, S., Liu, Z., Li, J., Wang, Y., Ma, Y., Sheng, L., Liu, H., Liang, F., Xin, G., and Wang, J.: Numerical simulation for the coupling effect
30   of local atmospheric circulations over the area of Beijing, Tianjin and Hebei Province, Science in China Series D: Earth Sciences, 52, 382–392, 2009.

Mader, P. P., MacPhee, R. D., Lofberg, R. T., and Larson, G. P.: Composition of organic portion of atmospheric aerosols in the Los Angeles area, Industrial & Engineering Chemistry, 44, 1352–1355, 1952.

Meng, Y. and Cheng, C.: Analyses of surface weather patterns for influencing air pollutants in Beijing area, Meteorology, 28(4), 42–47, 2002.

35 Parrish, D. D., Singh, H. B., Molina, L., and Madronich, S.: Air quality progress in North American megacities: A review, Atmos. Environ., 45, 7015–7025, 2011.

Putaud, J.-P., Raes, F., Van Dingenen, R., Brüggemann, E., Facchini, M.-C., Decesari, S., Fuzzi, S., Gehrig, R., Hüglin, C., Laj, P., et al.: A European aerosol phenomenology-2: Chemical characteristics of particulate matter at kerbside, urban, rural and background sites in Europe, Atmos. Environ., 38, 2579–2595, 2004.

Putaud, J.-P., Van Dingenen, R., Alastuey, A., Bauer, H., Birmili, W., Cyrys, J., Flentje, H., Fuzzi, S., Gehrig, R., Hansson, H.-C., et al.: A European aerosol phenomenology–3: Physical and chemical characteristics of particulate matter from 60 rural, urban, and kerbside sites across Europe, Atmos. Environ., 44, 1308–1320, 2010.

Quan, J., Tie, X., Zhang, Q., Liu, Q., Li, X., Gao, Y., and Zhao, D.: Characteristics of heavy aerosol pollution during the 2012–2013 winter in Beijing, China, Atmos. Environ., 88, 83–89, 2014.

Sun, F., Zhang, D., Sun, R., Dong, X., Wang, X., Wang, Z., and Cheng, N.: Case analyses of typical winter PM2.5 pollutions in Beijing, Environment Monitoring in China (in Chinese), 30, 1–12, 2014.

Sun, J., Desjardins, R., Mahrt, L., and MacPherson, I.: Transport of carbon dioxide, water vapor, and ozone by turbulence and local circulations, J. Geophys. Res., 103, 25 873–25 885, 1998.

Sun, J., Lenschow, D. H., LeMone, M. A., and Mahrt, L.: The role of large-coherent-eddy transport in the atmospheric surface layer based on CASES-99 observations, Boundary-Layer Meteorol., 160(1), 83–111, https://doi.org/10.1007/s10546-016-0134-0, 2016.

Sun, J., Cheng, Z., Li, J., Dou, J., Cao, X., Zhang, J., and Zhou, M.: Influences of urban canopies on turbulent mixing in the lower atmospheric boundary layer, J. Appl. Meteor. Clim., 2017.

Van Dingenen, R., Raes, F., Putaud, J.-P., Baltensperger, U., Charron, A., Facchini, M.-C., Decesari, S., Fuzzi, S., Gehrig, R., Hansson, H.-C., et al.: A European aerosol phenomenology-1 : Physical characteristics of particulate matter at kerbside, urban, rural and background sites in Europe, Atmos. Environ., 38, 2561–2577, 2004.

Wang, Y., Yao, L., Wang, L., Liu, Z., Ji, D., Tang, G., Zhang, J., Sun, Y., Hu, B., and Xin, J.: Mechanism for the formation of the January 2013 heavy haze pollution episode over Central and Eastern China, Science China Earth Sciences, 57, 14–25, 2014a.

Wang, Z., Li, J., Wang, Z., Yang, W., Tang, X., Ge, B., Yan, P., Zhu, L., Chen, X., Chen, H., et al.: Modeling study of regional severe hazes over Mid-Eastern China in January 2013 and its implications on pollution prevention and control, Science China Earth Sciences, 57, 3–13, 2014b.

Xu, X., Zhou, X., and Shi, X.: Characteristics of spatial structures and scale analyses of air pollution over urban areas, Sinica D. Geophysics, 35(S1), 1–19, 2005.

Zhang, B., Liu, S., and Liu, H.: Differences of MYJ and YSU in WRF on atmospheric boundary layer simulations, Geophysics Report, 55(7), 2239–2248, 2012.

Zhang, K., Cai, X., and Chai, F.: Analyses of fall characteristics and structures of the atmospheric boundary layer at Beijing, Peking University Technical Report of Natural Science, 42, 220–225, 2006.

Zhang, R., Wang, G., Guo, S., Zamora, M. L., Ying, Q., Lin, Y., Wang, W., Hu, M., and Wang, Y.: Formation of urban fine particulate matter, Chemical Reviews, 115, 3803–3855, 2015.

Zhang, W., Guo, J., Sun, Y., Yuan, H., Zhuang, G., Zhuang, Y., and Hao, Z.: Source apportionment for urban PM10 and PM2.5 in the Beijing area, Chinese Science Bulletin, 52, 608–615, 2007.

Zhao, X., Zhao, P., Xu, J., Meng, W., Pu, W., Dong, F., He, D., and Shi, Q.: Analysis of a winter regional haze event and its formation mechanism in the North China Plain, Atmos. Chem. Phys., 13, 5685–5696, 2013.
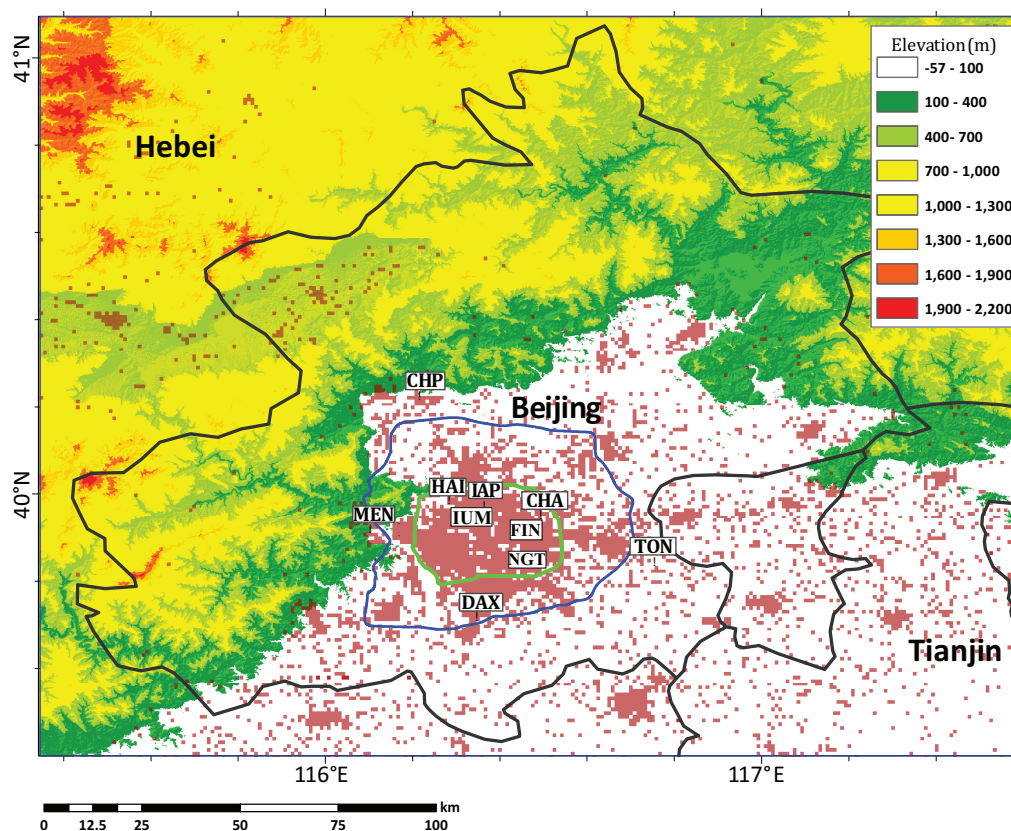
Figure 1. Map of topography around Beijing (bounded by the black curve with "Beijing" in its center), China, where the building areas (brown dots), the 6th (blue curve) and the 5th (green curve) ring roads, and the main observation sites used in this study are marked.
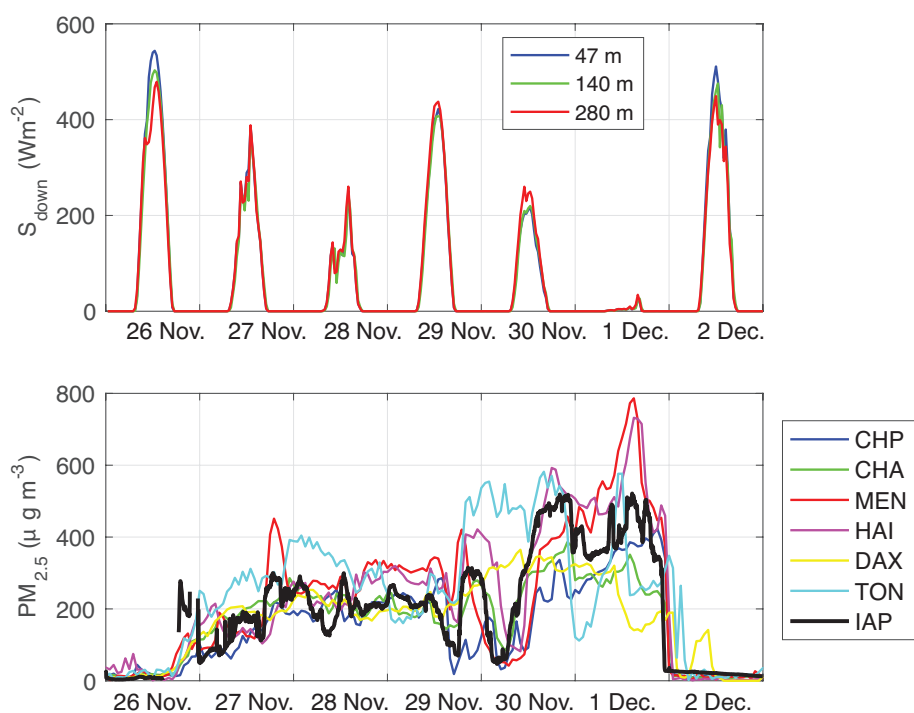
Figure 2. (a) The downward solar radiation S_{down} and (b) the temporal variation of the $PM_{2.5}$ concentration at the labeled stations.
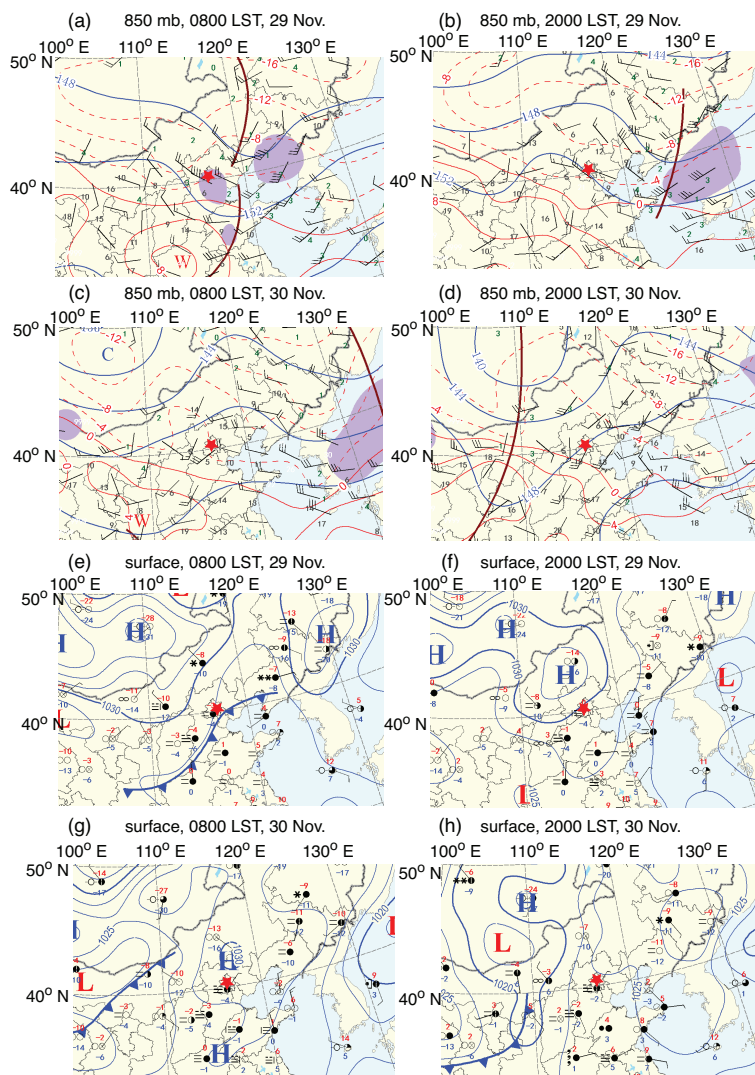
Figure 3. The 850-mb weather maps at (a) 0800 LST and (b) 2000 LST, and the surface maps at (c) 0800 LST and (d) 2000 LST on 30 November, where Beijing is marked by the red star in each panel.
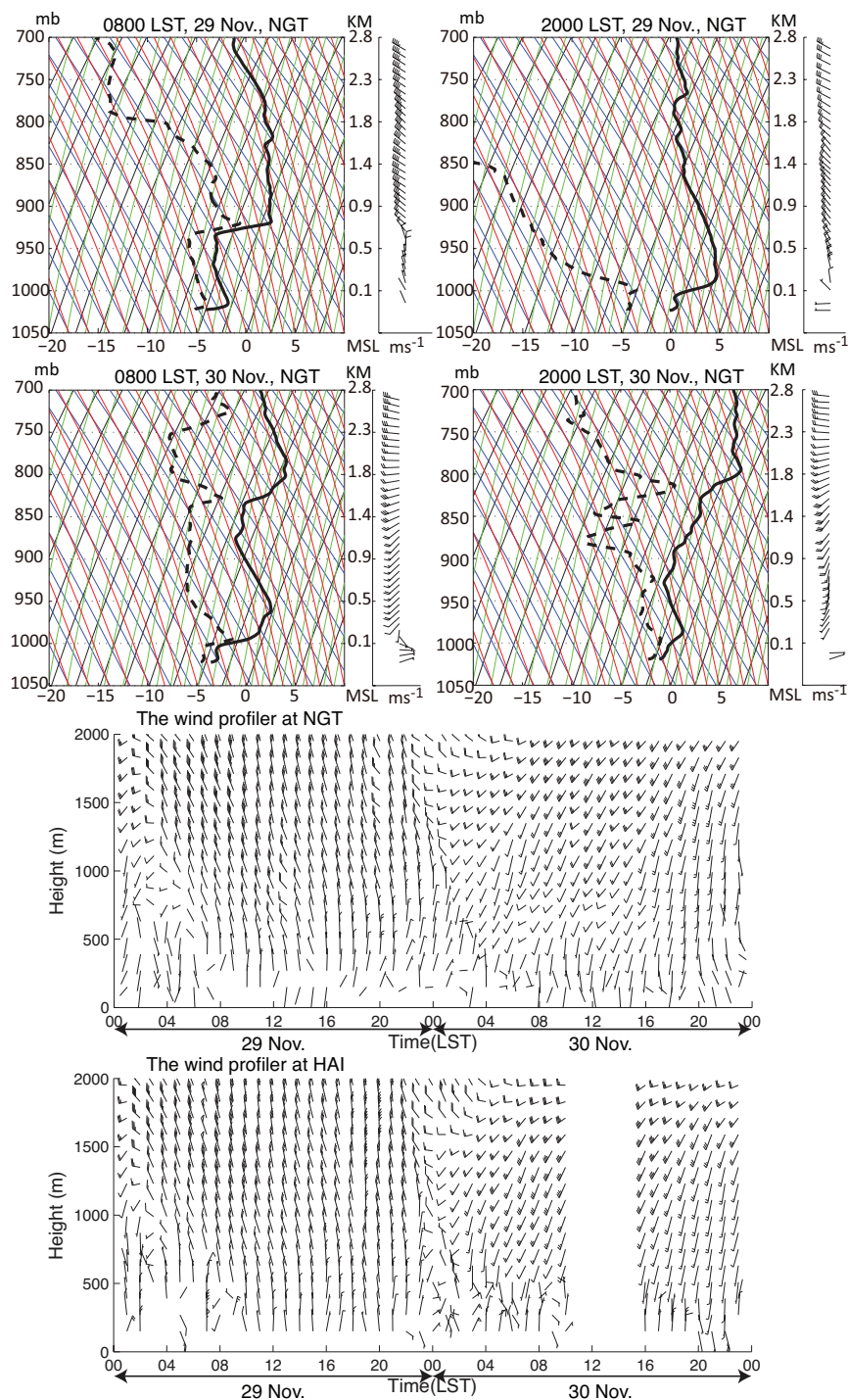
Figure 4. Temperature (solid), dew point (dashed), and wind vectors from the sounding profiles at 0800 LST and 2000 LST at NGT on 29 (top row) and 30 (the top second tow) November, and the temporal variation of the hourly wind-vector profiles from the wind profiler at NGT (the top third row) and at HAI (bottom) for 29-30 November.
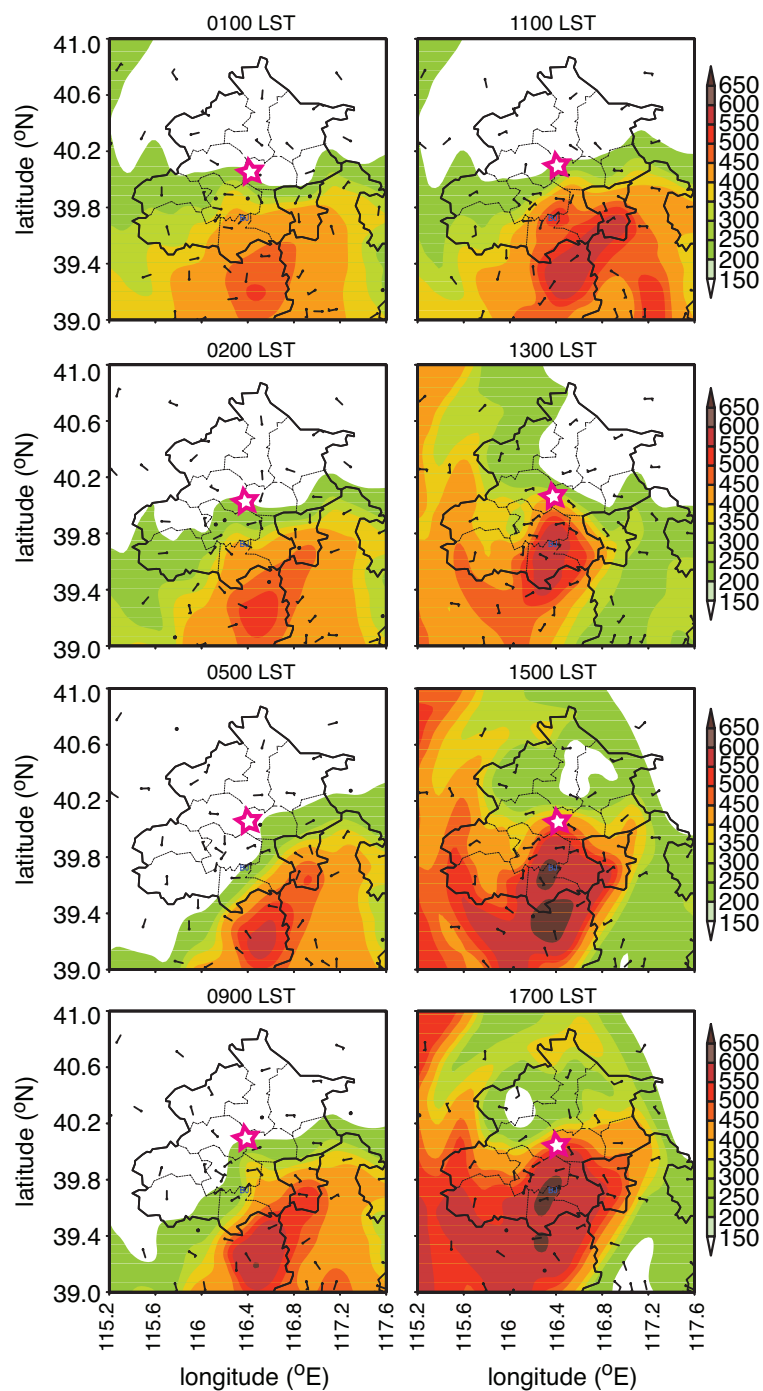
Figure 5. The PM$_{2.5}$ concentration at 0000 LST, 0200 LST, 0500 LST, 0900 LST, and 1100 LST, 1300 LST, 1500 LST, and 1700 LST on 30 November with surface wind barbs. The Beijing city boundary is marked by the dark black curve with the magenta star in its center.
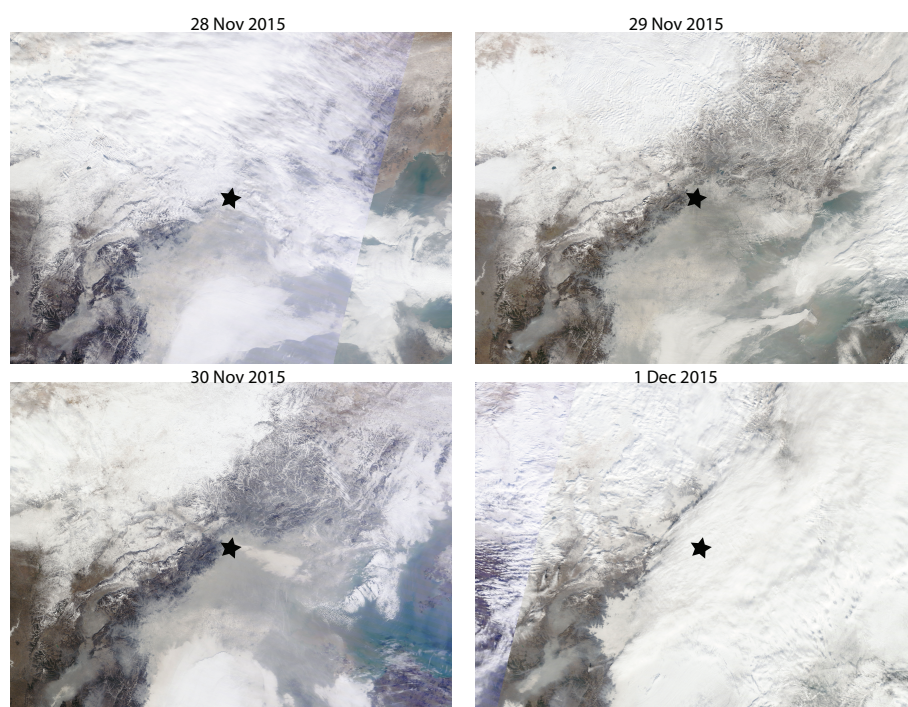
Figure 6. MODIS rapid response images around noon from 28 November to 1 December, 2015, where the star marked the location of Peking University, Beijing, China. The dark line southwest of the star visible on the images of 28, 29 and 30 November is the Taihang Mountain Ridge.
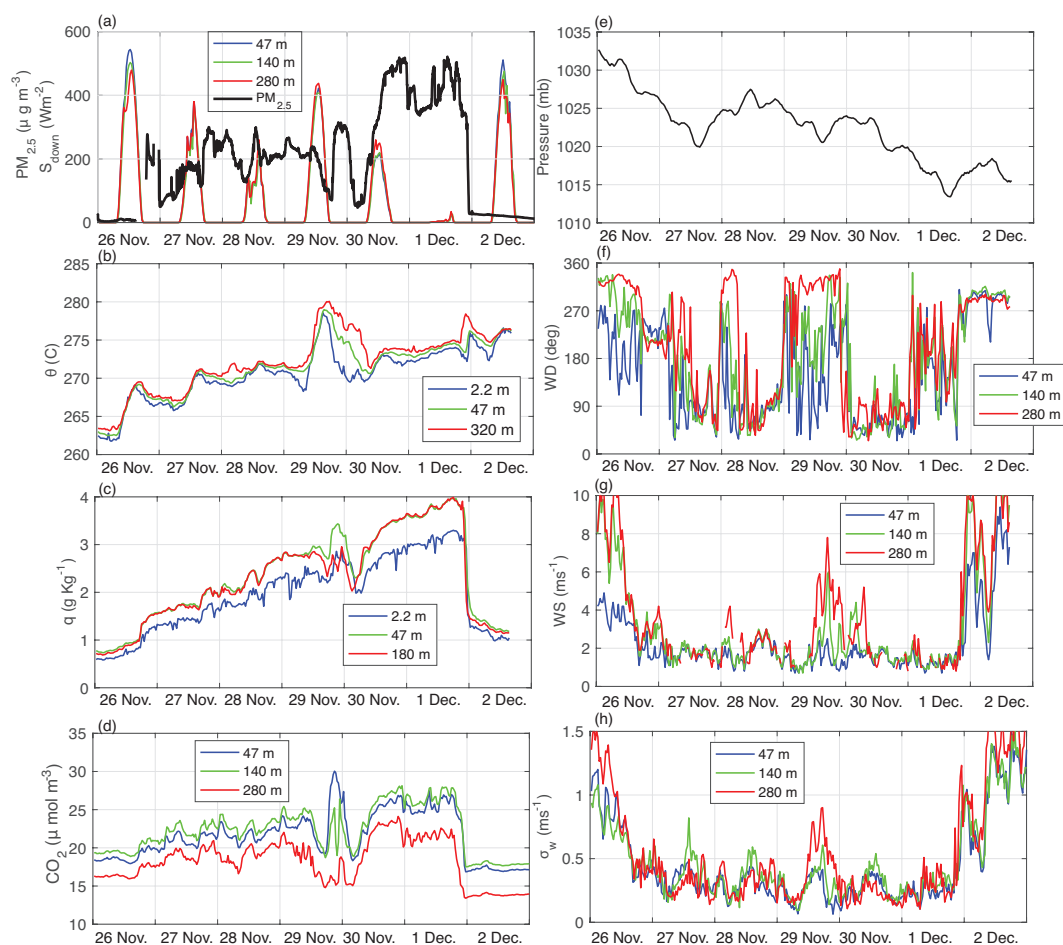
Figure 7. Temporal variations of (a) the PM$_{2.5}$ concentration and the downward solar radiation S_{down}, (b) the potential temperature θ, (c) the specific humidity, (d) the CO$_2$ concentration, (e) the pressure at 2.2 m, (f) wind direction WD, (g) wind speed WS, and (h) the standard deviation of the vertical velocity σ_w at IAP from 26 November to 2 December.
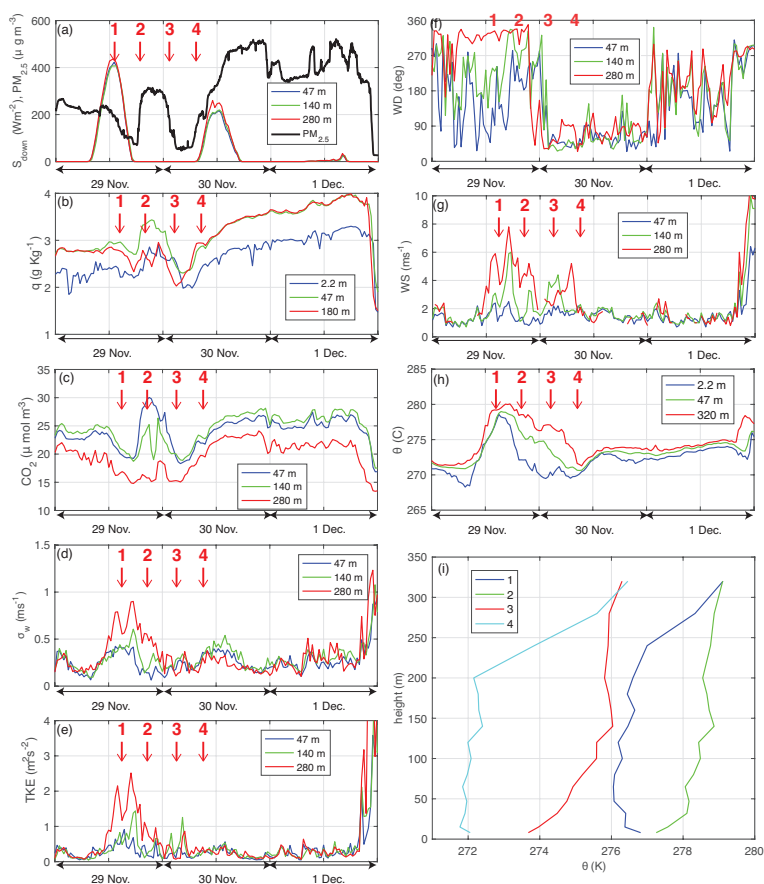
Figure 8. Temporal variations of (a) the $PM_{2.5}$ concentration and the downward solar radiation S_{down}, (b) the specific humidity, (c) the CO_2 concentration, (d) the standard deviation of the vertical velocity σ_w, (e) turbulence kinetic energy (TKE), (f) wind direction WD, (g) wind speed WS, (h) the potential temperature θ at IAP from 29 November to 1 December, and (i) θ profiles from the tower at the four times marked in (a)-(h).
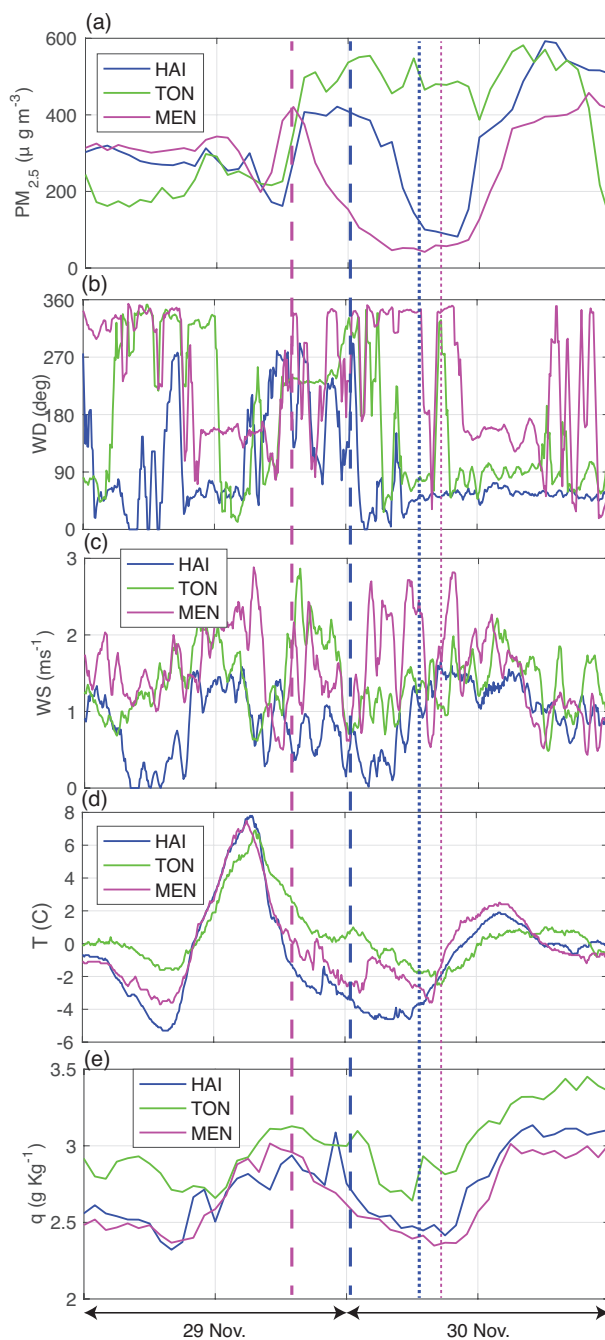
Figure 9. Temporal variations of (a) the $PM_{2.5}$ concentration, (b) wind direction WD, (c) wind speed (WS), (d) air temperature T, and (e) water vapor specific humidity q at Haidian (HAI), Tongzhou (TON) and Mentougou (MEN) from 29 to 30 November. The vertical dashed lines with the corresponding colors for MEN and HAI mark the $PM_{2.5}$ decreases (stage 3) associated with the wind speed and direction changes as a results of interactions between the downslope wind and the weak northeasterly surface wind in the SBL. The vertical dotted lines mark the $PM_{2.5}$ increases (stage 4) associated with the development of the convective boundary layer at the two stations.
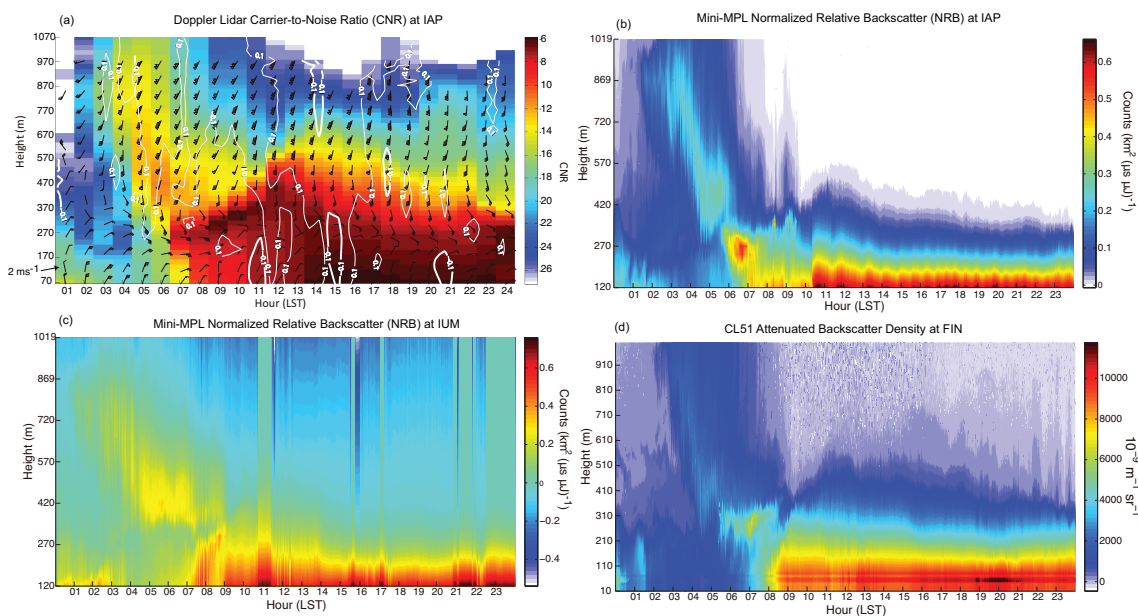
Figure 10. (a) The Doppler lidar carrier to noise ratio (CNR) with wind barbs at IAP, the normalized relative backscatter (NRB) from the mini-MPL lidar at (b) IAP and (c) IUM, and (d) the attenuated backscatter density from the CL51 lidar at FIN on 30 November. The wind barbs of 2 m s^{-1} is marked in (a).
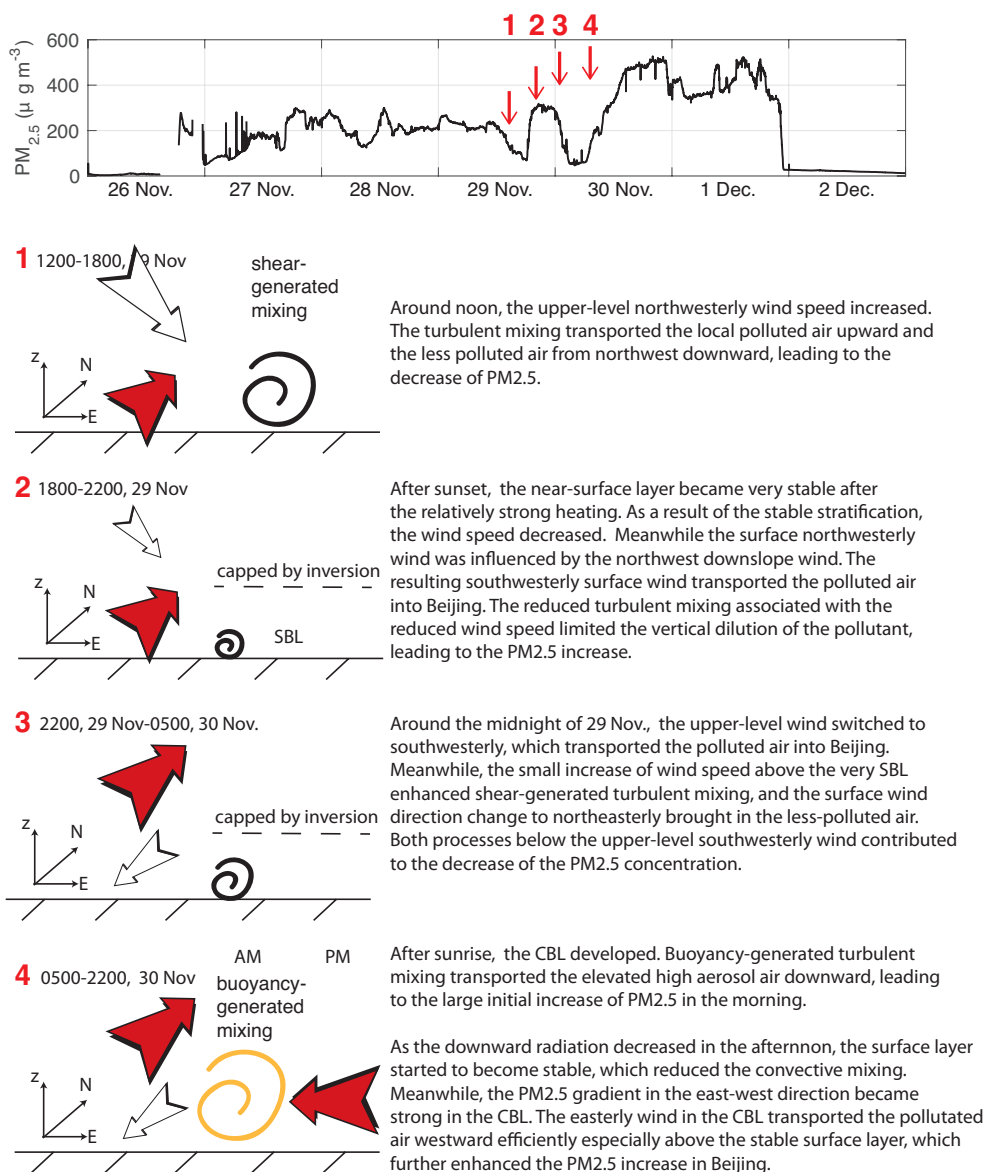
Figure 11. Schematic diagram of the roles of turbulent mixing and advection in the PM$_{2.5}$ oscillation prior to and in the development of the heavy pollution event on 30 November at IAP. Thermally and mechanically forced turbulence eddies are represented by yellow and black spirals. The white and the red arrows represent the relatively clean and dirty air, respectively.